# Ionospheric Dawnside Subauroral Polarization Streams: A Unique Feature of Major Geomagnetic Storms

Dong Lin[1], Wenbin Wang[2], Viacheslav G. Merkin[3], Chaosong Huang[4], Meers M. Oppenheim[5], Kareem Sorathia[3], Kevin H Pham[1], Adam Michael[6], Shanshan Bao[7], Qian Wu[8], Yongliang Zhang[3], Michael Wiltberger[8], Frank R. Toffoletto[7], John Lyon[9], and Jeffrey Garretson[10]

[1]National Center for Atmospheric Research
[2]HAO/NCAR
[3]The Johns Hopkins University Applied Physics Laboratory
[4]Air Force Research Laboratory
[5]Boston University
[6]The John Hopkins Applied Physics Laboratory
[7]Rice University
[8]National Center for Atmospheric Research (UCAR)
[9]Dartmouth College
[10]Johns Hopkins Applied Physics Lab

November 22, 2022

## Abstract

Strong subauroral plasma flows were observed in the dawnside ionosphere during the 20 November 2003 super geomagnetic storm. They are identified as dawnside subauroral polarization streams (SAPS) in which plasma drift direction is eastward and opposite to the westward SAPS typically found in the dusk sector. Both dawnside and duskside SAPS are driven by the enhanced meridional electric field in the low latitude portion of Region-2 field-aligned currents (FACs) in the subauroral region where ionospheric conductance is relatively low. However, dawnside eastward SAPS were only observed in the main and recovery phases while duskside westward SAPS were found much earlier before the sudden storm commencement. Simulations with the Multiscale Atmosphere-Geospace Environment (MAGE) model demonstrate that the eastward SAPS are associated with dawnside ring current build-up. Unlike the duskside where ring current build-up and SAPS formation can occur under moderate driving conditions, strong magnetospheric convection is required for plasmasheet ions to overcome their energy-dependent drifts to effectively build up the dawnside ring current and upward Region-2 FACs. We further used test particle simulations to show the characteristic drift pattern of energetic protons under strong convection conditions and how they are related to the dawnside SAPS occurrence. This study demonstrates the connection between the level of solar wind driving condition and a rare ionospheric structure, eastward SAPS on the dawnside, which only occur under strong convection typically associated with intense or super storms. Dawnside SAPS are suggested as a unique feature of major geomagnetic storms.

## Hosted file

`lin21_dawn_saps-sup-0001-supporting_information_si-s01_submit.docx` available at https://authorea.com/users/529967/articles/599107-ionospheric-dawnside-subauroral-polarization-streams-a-unique-feature-of-major-geomagnetic-storms

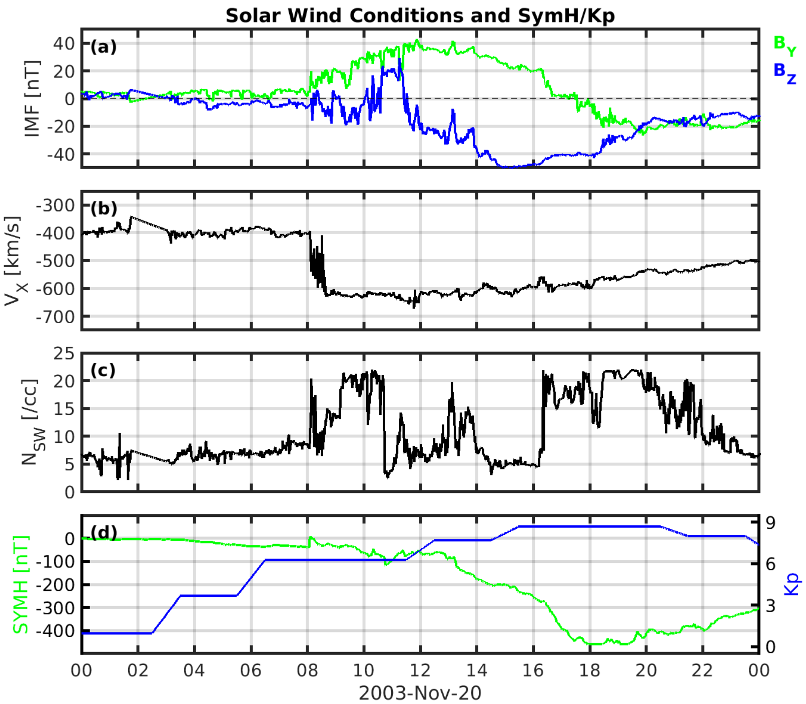
Solar Wind Conditions and SymH/Kp
(a)
IMF [nT]
$B_Y$
$B_Z$
(b)
$V_X$ [km/s]
(c)
$N_{SW}$ [/cc]
(d)
SYMH [nT]
Kp
2003-Nov-20

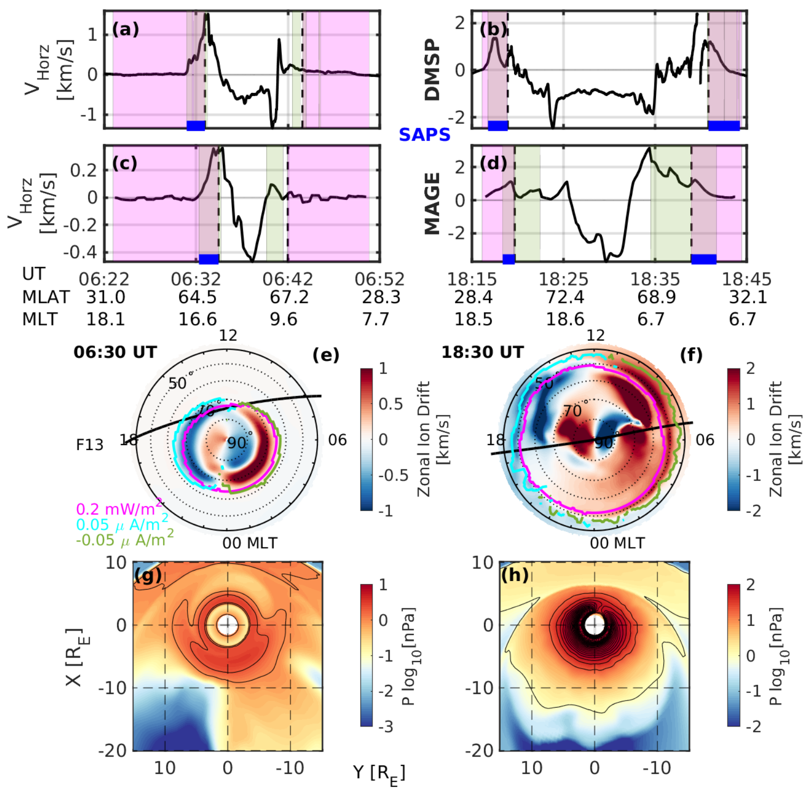
(a)
(b)
(c)
(d)
$V_{Horz}$ [km/s]
DMSP
SAPS
MAGE
UT 06:22 06:32 06:42 06:52
MLAT 31.0 64.5 67.2 28.3
MLT 18.1 16.6 9.6 7.7
18:15 18:25 18:35 18:45
28.4 72.4 68.9 32.1
18.5 18.6 6.7 6.7
06:30 UT
(e)
18:30 UT
(f)
F13
00 MLT
0.2 mW/m$^2$
0.05 $\mu$ A/m$^2$
-0.05 $\mu$ A/m$^2$
Zonal Ion Drift [km/s]
(g)
(h)
X [$R_E$]
Y [$R_E$]
P $\log_{10}$[nPa]

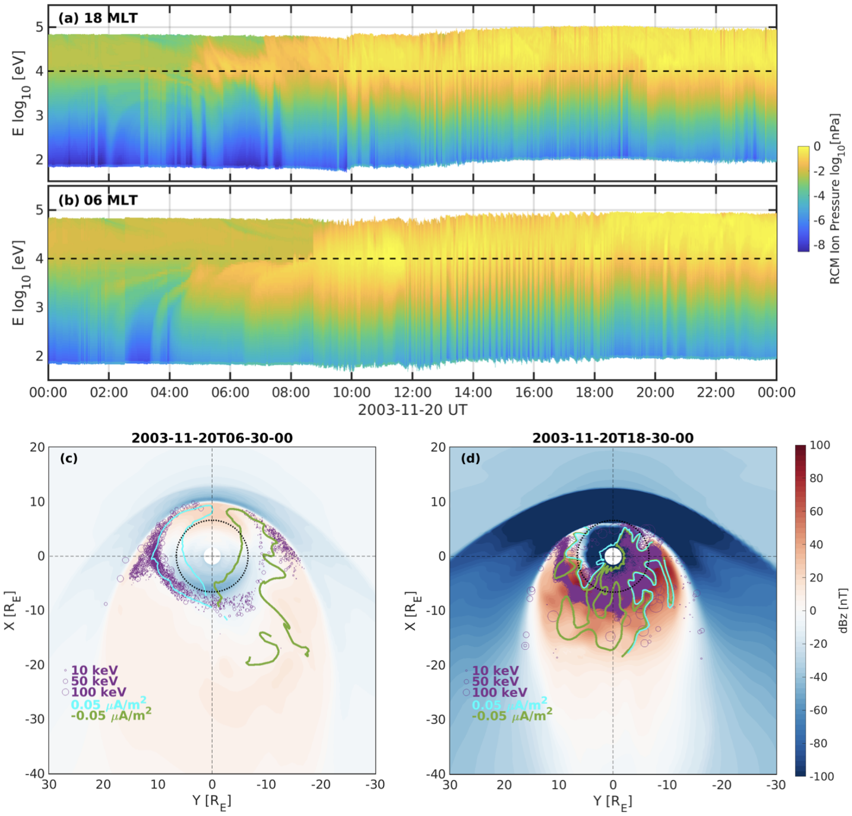

(a) 18 MLT
(b) 06 MLT
E log10 [eV]
RCM Ion Pressure log10[nPa]
2003-11-20 UT
00:00 02:00 04:00 06:00 08:00 10:00 12:00 14:00 16:00 18:00 20:00 22:00 00:00
2003-11-20T06-30-00
2003-11-20T18-30-00
(c)
(d)
10 keV
50 keV
100 keV
0.05 μA/m2
-0.05 μA/m2
X [RE]
Y [RE]
dBz [nT]

# Ionospheric Dawnside Subauroral Polarization Streams: A Unique Feature of Major Geomagnetic Storms

**Dong Lin[1], Wenbin Wang[1], Viacheslav Merkin[2], Chaosong Huang[3], Meers Oppenheim[4], Kareem Sorathia[2], Kevin Pham[1], Adam Michael[2], Shanshan Bao[5], Qian Wu[1], Yongliang Zhang[2], Michael Wiltberger[1], Frank Toffoletto[5], John Lyon[6], and Jeffrey Garretson[2]**

[1]High Altitude Observatory, National Center for Atmospheric Research, Boulder, CO
[2]Applied Physics Laboratory, Johns Hopkins University, Laurel, MD
[3]Space Vehicles Directorate, Air Force Research Laboratory, Kirtland AFB, NM
[4]Astronomy Department, Boston University, Boston, MA
[5]Department of Physics and Astronomy, Rice University, Houston, TX
[6]Department of Physics and Astronomy, Dartmouth College, Hanover, NH

**Key Points:**

- Dawnside SAPS with strong eastward subauroral ion flow are identified as a unique feature of major storms.
- The dawnside SAPS are associated with the storm-time strengthening of ring current pressure in the dawn sector.
- Energy-dependent ion drifts require strong convection to build up dawnside ring current and generate SAPS.

Corresponding author: Dong Lin, ldong@ucar.edu

**Abstract**

Strong subauroral plasma flows were observed in the dawnside ionosphere during the 20 November 2003 super geomagnetic storm. They are identified as dawnside subauroral polarization streams (SAPS) in which plasma drift direction is eastward and opposite to the westward SAPS typically found in the dusk sector. Both dawnside and duskside SAPS are driven by the enhanced meridional electric field in the low latitude portion of Region-2 field-aligned currents (FACs) in the subauroral region where ionospheric conductance is relatively low. However, dawnside eastward SAPS were only observed in the main and recovery phases while duskside westward SAPS were found much earlier before the sudden storm commencement. Simulations with the Multiscale Atmosphere-Geospace Environment (MAGE) model demonstrate that the eastward SAPS are associated with dawnside ring current build-up. Unlike the duskside where ring current build-up and SAPS formation can occur under moderate driving conditions, strong magnetospheric convection is required for plasmasheet ions to overcome their energy-dependent drifts to effectively build up the dawnside ring current and upward Region-2 FACs. We further used test particle simulations to show the characteristic drift pattern of energetic protons under strong convection conditions and how they are related to the dawnside SAPS occurrence. This study demonstrates the connection between the level of solar wind driving condition and a rare ionospheric structure, eastward SAPS on the dawnside, which only occur under strong convection typically associated with intense or super storms. Dawnside SAPS are suggested as a unique feature of major geomagnetic storms.

## Plain Language Summary

Subauroral polarization streams (SAPS) are typically defined as westward plasma flows equatorward of the auroral boundary on the duskside. They are usually observed in the downward Region-2 field-aligned currents from postnoon to premidnight where the ionospheric conductance is low in the mid-latitude ionospheric trough region. Similar SAPS structures were recently reported on the dawnside during a major storm event on 20 November 2003 where the subauroral plasma flew eastward and was associated with upward Region-2 FACs. While the dawnside subauroral plasma flows can be explained with a similar mechanism as their duskside counterpart, it is interesting to note that duskside SAPS occur much earlier and have been reported much more often than the dawnside SAPS. This study uses a state-of-the-art geospace model called MAGE (Multiscale Atmosphere-Geospace Environment) and satellite observations to investigate why it is easier for the duskside SAPS to occur. We found the dawnside SAPS are directly related to strong convection in major storms, which is required for protons to overcome their energy-dependent drift to substantially build up the dawnside ring current pressure and consequently, upward Region-2 field-aligned currents and eastward SAPS in the dawn. This rare signature is suggested as a unique feature of major storms.

## 1 Introduction

Subauroral polarization streams (SAPS) typically refer to an enhanced westward, latitudinally narrow plasma flow channel in the duskside subauroral ionosphere. SAPS are an important process in magnetosphere-ionosphere-thermosphere coupling because their distribution and variability result from processes on the auroral equatorward boundary, plasmasheet and ring current inner boundaries, and plasmapause, where complex interactions occur among the solar wind, magnetosphere, and ionosphere-thermosphere. SAPS have been widely observed by incoherent scattering radars, satellites such as the Defense Meteorology Satellite Programs (DMSP), and SuperDARN high frequency radars (e.g., ?, ?, ?, ?, ?, ?). ? (?) found that SAPS span from dusk to the early morning sector for Kp greater than 4. SAPS in the post-midnight to dawn sectors have an average peak speed of 400 m/s in the westward direction. ? (?) investigated the occurrence of

SAPS during intense storms with DMSP measurements. They found that most of the SAPS are first generated near the dusk region during intense storms, where the azimuthal pressure gradient of the ring current peaks and strong Region-2 FACs are generated. ? (?) found with SuperDARN and DMSP data that SAPS tend to be localized to the midnight sector during relatively quiet conditions. As the geomagnetic activity level increases, the peak location of SAPS shifts equatorward and duskward. ? (?) also found that SAPS have the maximum speed and width at 18-20 magnetic local time (MLT) based on DMSP observations. The statistical analysis of ? (?) showed that SAPS channels have a higher peak velocity and a broader latitudinal width in the dusk to midnight sector (17-21 MLT) than in the midnight sector (22-02 MLT). Various data sources have revealed that SAPS occur mostly in the dusk sector although the westward SAPS flow channel may extend to the post-midnight and dawn sectors during strong geomagnetic activities.

The preponderance of SAPS on the duskside is related to their fundamental driving mechanisms, which have been established in the past studies (e.g., ?, ?, ?, ?, ?). SAPS occur below the equatorward electron auroral boundary where the ionospheric conductance is relatively low but there are still finite downward field-aligned currents (FACs) in the low latitude portion of the Region-2 FACs. Since the Region-2 FACs are downward on the duskside (?, ?), the current closure requirement results in an enhanced poleward electric field which drives the westward fast SAPS plasma flow. The Region-2 FACs are mainly driven by the azimuthal pressure gradient in the ring current (e.g., ?, ?), which is known to be dawn-dusk asymmetric with the duskside current being stronger (e.g., ?, ?, ?, ?). It is, therefore, not surprising that the SAPS occur predominantly on the duskside and flow westward.

Recently, ? (?) and ? (?) used DMSP measurements to analyze the magnetosphere-ionosphere-thermosphere coupling during the 20 November 2003 super storm and found sunward plasma flows in the dawnside subauroral region. The eastward subauroral plasma flows were termed dawnside SAPS. The dawnside SAPS are explained by a similar mechanism of current closure to that of the duskside SAPS, except that the directions of the dawnside meridional electric field, FACs and plasma flow are opposite to those on the dusk side. However, critical questions remain to be answered. Are the dawnside SAPS driven by the same physical causes of the duskside SAPS? Is the occurrence comparable between the dawnside and duskside? Are the driving processes similar? How do the ring current build up and Region-2 FACs strengthen on the dawnside during the storm and lead to the generation of the eastward SAPS? Why were dawnside SAPS not reported in previous studies of the subauroral convection? What is unique and general about dawnside SAPS in this specific storm on 20 November 2003?

These questions are also critical to understanding magnetosphere-ionosphere coupling, especially on the dawnside which has drawn less attention compared to the duskside. ? (?) reported a double partial ring current pattern in both the premidnight and postmidnight quadrants during the main phase of storms, based on a large data set of magnetic field measurements in the magnetosphere. It was conjectured to be an integral effect of transient eastward currents associated with the substorm current wedge (SCW) or a distinct cold dense ion population in the postmidnight sector. ? (?) inferred that a current wedge structure exists on the dawnside based on ground magnetometer measurements during the same November 2003 super geomagnetic storm and several another intense and super storms. The dawnside current wedge was attributed to the eastward expansion of the intensified westward auroral electrojet, which was interpreted as a result of magnetotail dipolarization on the dawnside and tail current reduction. ? (?) further found a correlation between the dawn-dusk asymmetry of ground magnetic perturbation and the dawnside westward auroral electrojet. The dawnside current wedge was suggested as a distinct constituent of the storm time magnetospheric current system. However, the development of the dawnside current system during storm times and its connection to the dawnside SAPS have not been examined in detail.

In this study, we revisit the super geomagnetic storm on 20 November 2003 by comparing the dawnside and duskside and comparing the activities before the storm started and during the main and recovery phases. Besides observational analysis of DMSP measurements, we also use the newly developed Multiscale Atmosphere-Geospace Environment (MAGE) model, which has been demonstrated to have the necessary capability to resolve the mesoscale SAPS structures and self-consistently characterize the magnetosphere-ionosphere coupling (?, ?). We interpret the driving processes of the dawnside SAPS from DMSP measured auroral precipitation, ionospheric ion drift, and magnetic perturbation signatures, with the aid of MAGE simulation results. Comparisons between the dawnside and duskside, and between different stages of the storm, are made to understand the characteristic behaviors of ring current ions, i.e. they require strong convection to access the dawnside and strengthen the ring current and upward Region-2 FACs there, which are critical for the formation of dawnside SAPS. The featuring dependence on magnetospheric convection is illustrated with test particle simulations and suggested as an exclusive feature for major geomagnetic storms.

## 2 Model setup

MAGE is a newly developed geospace model that was designed in particular to resolve and study mesoscale structures, such as SAPS (?, ?) during storms. The current version of MAGE consists of the Grid Agnostic MHD with Extended Research Applications (GAMERA) global MHD model of the magnetosphere (?, ?, ?), the Rice Convection Model (RCM) model of the ring current (?, ?), Thermosphere Ionosphere Electrodynamics General Circulation Model (TIEGCM) of the upper atmosphere (?, ?), and RE-developed Magnetosphere-Ionosphere Coupler/Solver (REMIX) (?, ?). GAMERA is a new MHD model based on the algorithms underlying the high-heritage, the Lyon-Fedder-Mobbary (LFM) model (?, ?). Furthermore, MAGE carries on the legacy of the previous coupled geospace model developed by the same group (e.g., ?, ?) but is based on an entirely new coupling infrastructure.

In this study, MAGE uses a high grid resolution sufficient to resolve the mesoscale structures of SAPS. Specifically, GAMERA uses $96 \times 96 \times 128$ grid cells in the radial, meridional, and azimuthal directions, respectively, where the spherical symmetry axis of the grid is pointing from Earth to Sun. The grid spacing is $\sim 0.2\ R_E$ near the inner boundary, which is set at 1.5 $R_E$. RCM uses $180 \times 360 \times 115$ grid cells in the latitudinal, longitudinal (in Solar Magnetic, SM, coordinates), and energy dimensions, respectively. The RCM grid has a resolution of 0.25° in latitude and 1° in longitude. In the energy dimension, there are 29 energy channels for electrons, 85 energy channels for protons, and 1 zero-energy channel for the cold plasmasphere. REMIX grid uses 55 x 360 grid cells in the latitudinal and longitudinal directions (in SM), respectively. Its resolution is 1.0° in both dimensions and the low latitude boundary is at 35° magnetic latitude (MLAT). TIEGCM uses $288 \times 144 \times 57$ cells in longitudinal, latitudinal, and altitudinal directions (in geographic coordinate system), respectively. It has a uniform horizontal resolution of 1.25° and a vertical pressure grid of 0.25 scale height. GAMERA and TIEGCM both adopt a ring-average technique to treat the singularity at the spherical axes of their respective grids (?, ?, ?). GAMERA and RCM exchange information every 10 s, GAMERA and REMIX every 5 s, and REMIX and TIEGCM every 5 s.

Figures 1a-1d show the solar wind/interplanetary magnetic field (IMF) conditions and SYMH/Kp indices during 20 November 2003. The data were obtained from the CDAWeb OMNI data base. The solar wind and IMF data were used to drive the MAGE model. A coronal mass ejection (CME) arrived at the Earth at around 08 UT on 20 November 2003. The solar wind speed was over 600 km/s for the next 8 hours. Strong IMF started to impact the magnetosphere with negative $B_Z$ as large as -20 nT in the first two hours after the sudden storm commencement and dropped to -50 nT by 15 UT. The SYMH

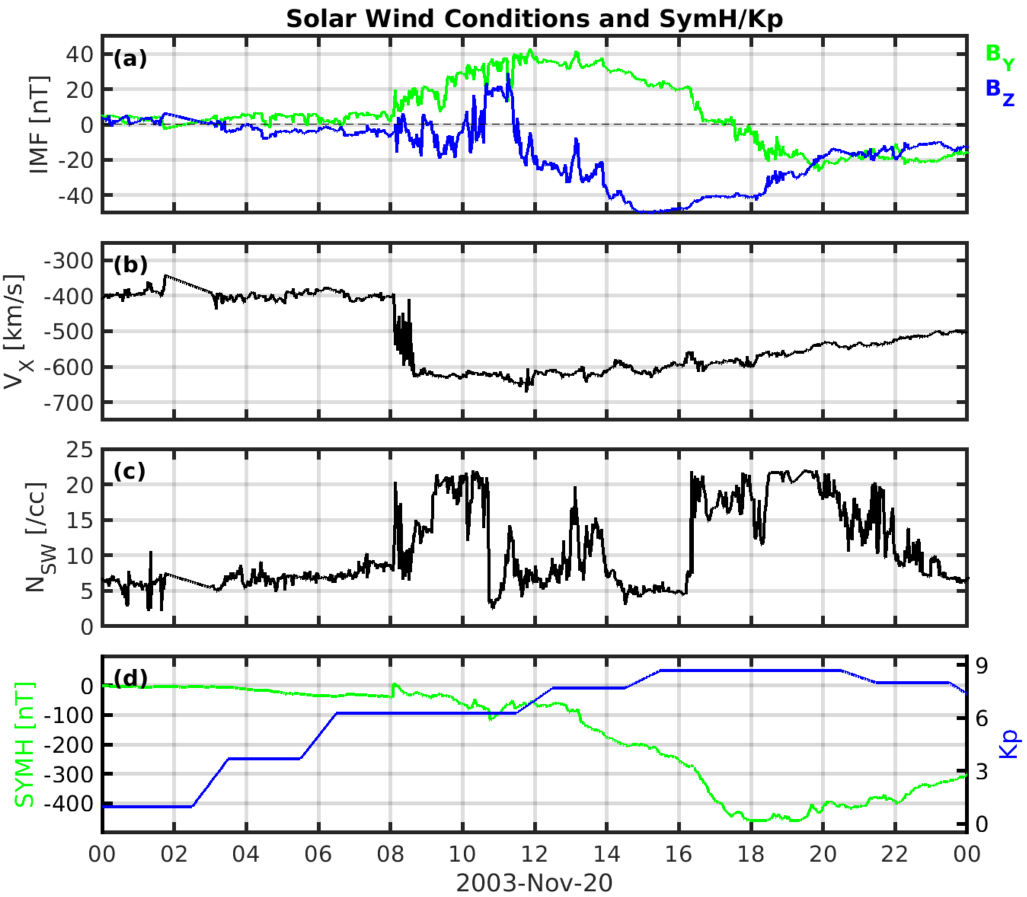


**Figure 1.** Solar wind/IMF and SYMH/Kp indices during 20 November 2003. (a) IMF $B_Y$ (green) and $B_Z$ (blue) in GSM coordinate. (b) Solar wind velocity $V_X$. (c) Solar wind density. (d) SYMH (green) and Kp indices (blue).

index reached a minimum of -457 nT at around 18 UT after which it gradually recovered.

# 3 Observations and simulation results

## 3.1 Structure of dawnside SAPS

Figures 2a-2e show an example of SAPS observed by the DMSP F16 satellite during its crossing of the northern hemisphere high-latitude ionosphere from 13:51 UT to 14:31 UT. From top to bottom are DMSP measurements of electron precipitation energy spectrum, integrated electron precipitation energy flux ($EnFlux$), cross-track ion drift velocity ($V_{HORZ}$), electron density, cross-track magnetic perturbation ($dB_Z$), and the derived FAC density. The data are smoothed with a 15 s moving mean window to show structures on the scale of over ~100 km. The vertical dashed lines show when $EnFlux$ drops to 0.2 $mW/m^2$ and are used to indicate the equatorward electron precipitation boundaries. Subauroral regions equatorward of those boundaries and poleward of 35° MLAT are shaded with the magenta color. FAC densities are calculated from $dB_Z$ by using Ampere's Law, assuming a current sheet (e.g., ?, ?, ?, ?). In the northern hemisphere, downward FACs are positive and upward FACs are negative. The green shaded regions highlight the upward FACs on the dawnside and downward FACs on the duskside, which are Region-2 currents. The FAC boundaries are estimated with a threshold value of 0.05 $\mu A/m^2$. Note that the FACs show alternating upward and downward signatures on the duskside, which imply finer structures embedded in the large-scale Region-1/Region-2 FACs (e.g., ?, ?, ?). Small scale FAC structures away from the equatorward auroral boundaries are not shaded for better visibility.

Figure 2c shows a separate sunward (westward) ion drift channel on the duskside around 13:58 UT with a peak value of nearly 1.6 km/s, marked with the thick blue horizontal bar. This is the typical duskside SAPS structure that has been widely observed and studied. Figure 2d shows an electron density trough collocated with the duskside SAPS channel and residing in the low-latitude portion of the downward Region-2 FACs. More interestingly, there is also a strong plasma flow channel on the dawnside below the equatorward boundary of electron aurora at about 56° MLAT. This flow channel has a magnitude of up to 1 km/s in the sunward/eastward direction. These dawnside flow structures are similar to those on the dusk side and hereinafter referred to as the dawnside SAPS. Note ? (?) showed several examples of dawnside SAPS observed by DMSP F13 only. Here we have examined all available DMSP data on 20 November 2003 and confirm that dawnside SAPS were detected by multiple DMSP satellites. The dawnside SAPS are also collocated with the low-latitude part of Region-2 FACs, which are upward on the dawnside. Note the electron density data on the dawnside does not show an apparent low-density trough structure. This is probably the reason that the flow speed of the dawnside SAPS channel is relatively smaller than that on the duskside and that the dawnside SAPS channel does not show a distinct peak as the dusk SAPS channel does. The rest of this paper will investigate the formation of the dawnside SAPS and their similarities to and differences from the duskside SAPS.

Figures 2f-2j show that both the dawn and dusk SAPS structures are captured by the MAGE model along the auroral crossing path of DMSP F16 during the same interval. Figures 2f-2h show the model outputs of $EnFlux$, $V_{HORZ}$, and FAC density sampled along the DMSP F16 trajectory. The sampled simulation results are also smoothed with a 15 s moving mean to remove subgrid fluctuations. Using a similar format in Figure 2b, Figure 2g shows a duskside SAPS flow channel at $\sim$ 19.5 MLT and $\sim 50°$ MLAT with a peak speed of $\sim$ 1.2 km/s. On the dawnside, a separate SAPS channel is visible at around 8.6 MLT and $\sim 54°$ MLAT, with a peak speed of $\sim$ 1.0 km/s. Both the duskside and dawnside SAPS channels are collocated with the low latitude part of Region-2 FACs, which are downward on the duskside and upward on the dawnside.

Note the simulated integrated electron precipitation energy flux on the dawnside is more than 20 $mW/m^2$, which is obviously overestimated compared to DMSP measurements. This is attributed to the electron precipitation model used in this MAGE simulation, where a uniform and constant electron loss rate is applied when deriving the diffuse electron precipitation. However, the overestimated electron precipitation should not affect the dawnside SAPS fundamentally except introducing a latitudinal minimum in $V_{HORZ}$. The equatorward electric field that drives the eastward subauroral flow is determined by the large scale of upward Region-2 FACs which requires closing via equatorward Pedersen currents from the downward Region-1 FACs at higher latitudes. However, it is noteworthy that a latitudinally local stronger precipitation energy flux generates a higher ionospheric conductance and hence a weaker equatorward electric field and a weaker eastward zonal drift, forming a separate flow channel like distribution.

Figures 2i and 2j show two-dimensional distributions of zonal ion drift at 13:57 UT and 14:22 UT in the northern hemisphere as viewed from above the north pole. DMSP F16 was located inside the duskside SAPS and dawnside SAPS at these two UTs, as indicated by the black circle and triangle, respectively. Here zonal drift is defined as positive for the eastward flow. The magenta curve shows the equatorward auroral boundary, which is identified by finding at each MLT where $EnFlux$ drops to below 0.2 $mW/m^2$. At 13:57 UT, a SAPS channel, i.e., enhanced plasma flow below the equatorward auroral boundary, can be seen on the duskside from 17 MLT to $\sim$ 22 MLT at around 50° MLAT, and on the dawnside from 0 MLT to about 10 MLT slightly above 50° MLAT.

Although they are not shown here, we checked other available DMSP satellite data at approximately the same time. DMSP F13 detected dawnside SAPS at 14:08 UT at $\sim$ 7.2 MLT and $\sim -59°$ MLAT and duskside SAPS at 14:29 UT at $\sim$ 18.4 MLT and $\sim -53°$ in the southern hemisphere. DMSP F14 detected dawnside SAPS at 14:19 UT at $\sim$ 8.2 MLT and $\sim -58°$ MLAT and duskside SAPS at 14:40 UT at $\sim$ 19.8 MLT and $\sim -53°$ MLAT in the southern hemisphere. DMSP F15 detected duskside SAPS at 13:48 UT at $\sim$ 20.9 MLT and $\sim$ 50° MLAT. But no obvious dawnside SAPS signatures were seen when DMSP F15 was crossing the dawnside northern hemisphere at 11 MLT. The locations where dawnside and duskside SAPS were detected by DMSP satellites are well within the range suggested by MAGE simulations. The above measurements by DMSP F13, F14, and F15 are provided in the Supporting Information as Figure S1, S2, and S3.

The generation processes of the duskside and dawnside are illustrated in Figures 2i and 2j by comparing the equatorward boundaries of electron precipitation and FACs. The equatorward electron precipitation boundary is shown by the magenta curve, which is identified by finding the latitude at each MLT where $EnFlux$ drops to below a threshold value of 0.2 $mW/m^2$. The cyan and green curves indicate the equatorward FAC boundaries at each MLT where FAC density drops to below 0.05 $\mu A/m^2$. The green curves show the equatorward boundary of upward FACs and the cyan curves show the equatorward boundary of downward FACs. The equatorward FAC boundaries are located at a lower latitude than the electron precipitation equatorward boundaries (magenta contours) on both the duskside and dawnside. As a result of current closure requirement, strong equatorward and poleward electric fields are produced in the low conductance subauroral regions, which drive eastward and westward SAPS on the dawnside and duskside, respectively.

It is also noteworthy, by comparing the two MAGE outputs at 13:57 UT and 14:22 UT in Figures 2i and 2j, that in just 25 minutes during the polar cap crossing of the virtual DMSP F16 satellite, the duskside SAPS channel extended toward the dayside to around 15 MLT. The dawnside SAPS channel also becomes much more prominent with a higher zonal drift velocity. The noticeable changes in high-latitude ion convection pattern during this period indicate the changes in solar wind/IMF driving conditions and the dynamic responses of the geospace system to changing driving conditions. Also note that the dawnside SAPS channel shows a clear separation from the auroral return flow from $\sim$ 2 MLT to 10 MLT. The distribution of a separate zonal flow channel suggests a strong latitudinal gradient in the meridional electric field, which results from a strong gradient in the ionospheric conductance and causally in the auroral precipitation.

### 3.2 Generation of dawnside SAPS

Figures 3a and 3b compare the SAPS structures detected by DMSP F13 in two orbits to understand their evolution during this storm. Figure 3a shows the cross track ion drift from 06:22 UT to 06:52 UT before the sudden storm commencement. SAPS already occur on the duskside but not the dawnside. The duskside equatorward auroral boundary, as shown by the vertical dashed line, was located at $\sim$ 66° MLAT when DMSP F13 crossed by. Downward Region-2 FACs of up to 0.5 $\mu A/m^2$ are derived from horizontal magnetic perturbations between $\sim$ 60° and $\sim 67^circ$, which are indicated by the green shaded region. Note here we only show the $V_{HORZ}$ data to focus on the SAPS structures as the analysis method has been demonstrated in Figure 2. A similar plot to 2 with detailed information of FAC and $EnFlux$ for the two crossing shown in Figure 3a-3d are provided in the Supporting Information as Figure S4-S7. Between the equatorward boundaries of electron precipitation and Region-2 FACs are SAPS plasma flows indicated by the blue horizontal bar, although they do not show a separate flow channel like shown in Figure 3b. On the dawnside, however, there is only a very narrow region of upward Region-2 FACs below the equatorward electron precipitation boundary, where the FAC density is only slightly above the threshold value of 0.05 $\mu A/m^2$. The $V_{HORZ}$ data also shows only negligible horizontal drifts. Therefore it is valid to claim no dawnside SAPS at around 6:30 UT before the sudden storm commencement.

Figure 3b shows $V_{HORZ}$ measured from 18:15 UT to 18:45 UT when the SYMH index was near its minimum. A separate SAPS channel is clearly visible on the duskside with a peak value of $\sim$ 1.2 km/s. The auroral boundary has moved equatorward by about 15° at this MLT of around 18. On the dawnside, a substantial eastward SAPS channel is also identifiable with a peak value of more than 1 km/s, similar to the one showed in Figure 2.

Figures 3c and 3d show the MAGE simulation results for the same two intervals. Similarly, SAPS already occurred on the duskside but not on the dawnside at around 6:30 UT. When it is deep in the main phase, substantial SAPS with peak values of more than 1 km/s are found on both the duskside and dawnside.

Both the DMSP data and MAGE simulation results reveal that the most important change related to the occurrence of dawnside SAPS was the location of the equatorward FAC boundary relative to the equatorward precipitation boundary. Figures 3e and 3f provide a more illustrative view of the SAPS evolution during the storm with MAGE simulated of zonal ion drifts at 06:30 UT and 18:30 UT, respectively. The format is similar to that in Figures 2i and 2j. Before the storm started, the upward Region-2 FAC boundary was very close to the auroral boundary on the dawnside. Refer to the green and magenta curves in Figure 3e. Therefore there were no SAPS formed there. When the storm activity level reached its peak, the upward Region-2 FAC boundary extended equatorward by several more degrees than the auroral boundary equatorward expansion, leaving dawnside SAPS formed in the gap between the two boundaries. Refer to the green and magenta curves again but also the red belt between the two boundaries representing the eastward SAPS channel.

The Region-2 FACs are mainly driven by the azimuthal pressure gradient in the inner magnetosphere (e.g., ?, ?). Figures 3g and 3h show the plasma pressure distributions in the magnetospheric equatorial plane on a logarithm scale at 6:30 UT and 18:30 UT, respectively. Note the color scale is one order of magnitude higher Figure 3h for 18:30 UT when the ring current pressure was significantly built up. The black curves are plasma pressure contours. In Figure 3g, the contour levels are separated by every 2 nPa, whereas in Figure 3h, the contour level separation is 20 nPa. The comparison of contour curves therefore shows an even more substantial increase in pressure gradient at 18:30 UT compared to 06:30 UT. In particular, the pressure gradient was greatly enhanced at almost all MLTs at 18:30 UT, which should account for the substantial strengthening of upward Region-2 FACs and occurrence of dawnside eastward SAPS at that stage.

### 3.3 Uniqueness of dawnside SAPS

Figure 4 compares the ring current partial pressure as a function of proton energy and UT between the dusk and dawn. The pressure is sampled at the geosynchronous orbit of $L = 6.6$ at 18 MLT and 06 MLT, respectively. Figure 4a shows that the duskside ring current pressure started to build up at around 5 UT when the IMF $B_Z$ turned southward. The total ring current pressure is dominantly contributed by protons with energies from 10 keV to 100 keV based on the RCM simulation results. This is consistent with the recent observational finding by ? (?) that the total ring current pressure comes mostly from energetic protons of 10-100 keV during the storm main phase and recovery phase. Note the energetic proton fluxes are overall enhanced at all energy levels, after $\sim 8$ UT due to the injections from the magnetotail. On the other hand, Figure 4b shows that the dawnside ring current pressure has a dramatic enhancement at 10-100 of keV since 8:45 UT when the solar wind speed jumped to more than 600 km/s. Statistically the magnetospheric convection becomes much stronger during the storm main phase (?, ?). Here we focus on the 10s keV protons because they are known to contribute significantly to the ring current energy content during storm time (?, ?).

The distinct responses of 10-100 keV energetic protons on the duskside and dawnside are responsible for the different occurrences of SAPS on the two sides. To better understand the dependence of energetic proton drifts on the strength of magnetospheric convection, we traced the trajectories of protons with a test particle model using the electromagnetic fields from the MAGE simulation. The test particle model used was the Conservative Hamiltonian Integrator of Magnetospheric Particles (CHIMP) model described in detail by ? (?) and ? (?). Protons with energies from 5 eV to 50 keV are released from the nightside equatorial plane between 21 MLT and 3 MLT at a radial distance between 14.5 $R_E$ and 15.5 $R_E$. In the two CHIMP runs, protons are released at 6 UT and 18 UT, when the magnetospheric convection was very weak before the sudden storm commencement and when it was greatly enhanced during the main phase, respectively.

Figures 4c and 4d show the distributions of test particle protons and background residual magnetic field $dB_Z$ with dipole subtracted in the equatorial plane 30 minutes after they were released. The purple circles represent protons that were active near the equatorial plane with the size of the circles proportional to the particle energy. The green and cyan curves indicate upward and downward FAC boundaries mapped from the northern hemisphere ionosphere. The boundaries are defined by a threshold FAC value of 0.05 $\mu A/m^2$.

In the first CHIMP simulation, protons released at 6 UT mostly drifted westward and were energized to the duskside. Figure 4c shows that a number of 10-100 keV protons were transported to inside the downward Region-2 FACs, the region enclosed by the cyan curve. However, the protons are rarely seen in the dawnside upward Region-2 FACs, the region enclosed by the green curve. In this case before the storm started, protons are dominated by their energy-dependent drift when the convection electric field was weak. That is why the dawnside ring current could not build up and Region-2 FACs were not sufficiently intensified to generate eastward SAPS.

In the second CHIMP simulation, protons released at 18 UT underwent a much stronger magnetospheric electric field. Proton motion was dominated by convection over energy dependent drifts. A significant amount of 100s keV protons are seen inside the dawnside geosynchronous orbit. These energetic protons occupied the region enclosed by solid green curves and were responsible for the ring current build-up and upward Region-2 FAC intensification on the dawnside, which ultimately drove the dawnside SAPS. The evolution of test particle protons in the two CHIMP runs are included in the Supporting Information as Movie S1 and S2.

The distribution of test particle protons is determined by their convection drift (?, ?). When the magnetospheric convection electric field is weak, typically during quiet times or weak to moderate storms, energy dependent gradient and curvature drift is dominant. Protons tend to drift westward to the duskside and build up the ring current pressure in the dusk sectors. When the convection is dominant, which corresponds to the situation during intense and super storms, the energy dependent drift is relatively negligible. Energetic protons have an easier access to the dawnside and deeper penetration under strong convection and corotation electric field. The convection dependent proton access to the inner magnetosphere, as predictable from adiabatic drift theory and illustrated with our test particle simulations, provides a valid explanation for the dawnside ring current build-up and Region-2 FAC intensification, which ultimately account for the formation of dawnside SAPS. More importantly, the dependence on magnetospheric convection and storm activity level makes the dawnside SAPS a unique feature that is only associated with strong geomagnetic storms.

## 4 Discussion

The comparison between 6:30 UT and 18:30 UT in Figure 3 indicates the importance of strong convection in the formation of dawnside SAPS. The dawnside SAPS were not noticed until recently by ? (?) probably because the required strong convection does not occur very often. During weak and moderate storms dawnside ring current build-up is less efficient so that they are not sufficient to produce noticeable dawnside SAPS. In a controlled MAGE experiment (not shown here), we artificially reduced all IMF components by a factor of ten while maintaining the same solar wind parameters. The reduce IMF has its strongest southward $B_Z$ of -5 nT, which qualifies as a weak storm condition. With greatly reduced magnetospheric convection, the duskside SAPS still occurred but the dawnside SAPS did not occur. The controlled experiment provides an additional support for the uniqueness of dawnside SAPS.

? (?) reported a list of major storms (Dst minimum ¡ -100 nT) in their analysis of dawnside intensification of auroral electrojet and FACs (Table 1 in (?, ?)). The events are featured by the ten largest hourly ground magnetic perturbations. We examined the DMSP data for these events. Dawnside SAPS were also found during those strong storm events except relatively weak signatures in the storm on 7 January 2005 which has a Dst minimum of -71 nT and should be classified as a moderate storm, and in the storm on 22 October 2001 which has a Dst minimum of -177 nT. A statistical survey of dawnside SAPS is necessary to better understand their occurrence with a more detailed description of their dependence on the storm activity level.

We also note that the IMF $B_Y$ was also very strong in the 20 November 2003 event. IMF $B_Y$ increased to a maximum of positive 40 nT at around 12 UT during the early main phase. A strong IMF $B_Y$ is known to cause substantial dawn-dusk asymmetries of the coupled magnetosphere-ionosphere, (e.g., ?, ?, ?, ?). We conducted another controlled experiment of MAGE simulation in which IMF $B_Y$ was artificially reduced to zero while other solar wind and IMF parameters were the observed values. The dawnside SAPS still occurred in this case despite a more dawn-dusk symmetric convection and FAC pattern. At 12 UT when the IMF difference was the largest between the two runs with original and artificially removed IMF $B_Y$, a separate channel of eastward subauroral flow appeared in the prenoon sector with a peak speed of $\sim 1$ km/s. Therefore IMF $B_Y$ was not the determining factor for the generation of dawnside SAPS.

It is necessary to clarify that the dawnside SAPS studied in this work are different from the recently reported dawnside polarization streams (DAPS) (? (?)). Both DAPS and dawnside SAPS occur on the dawnside and refer to the enhanced eastward plasma flows. But DAPS occur above the poleward auroral boundary inside the polar cap while dawnside SAPS occur equatorward of the auroral boundary at subauroral latitudes. DAPS are driven by the current closure of Region-1 FACs while dawnside SAPS are driven by the Region-2 FACs.

There have also been reports of eastward subauroral plasma flows, (e.g., ?, ?, ?, ?, ?), which are called abnormal SAPS or abnormal SAID. The eastward drifts and equatorward electric fields of abnormal SAPS were suggested to be associated with the so-called over-shielding effects, i.e. Region-2 FACs dominating over Region-1 FACs due to IMF northward turning or reduced convection under southward IMF. These abnormal cases occur in the dusk or premidnight sectors under relatively weak driving conditions and are thus different from the strong dawnside SAPS investigated in this study.

## 5 Conclusion

In this study we investigated the eastward subauroral plasma flow on the dawnside, i.e. dawnside SAPS, during the 20 November 2003 super storm. DMSP satellite observations and MAGE simulations reveal a similar driving mechanism between the dawnside and duskside SAPS, i.e., Region-2 FACs extend to equatorward of the low latitude auroral boundary. An strong equatorward electric field is required for current closure of the upward Region-2 FACs which drives the enhanced eastward flow. The comparison between the storm time and before the storm started reveals that strong magnetospheric convection is required for the dawnside ring current to build up and upward Region-2 FACs to intensify, which are critical to generate SAPS in the dawnside ionosphere. The dependence on a strong convection electric field, which typically represents the level of a geomagnetic storm, suggests that the dawnside SAPS is a unique feature of major geomagnetic storms.

## Data Availability Statement

The MAGE simulation data used for dawnside SAPS analysis in the study are available at the NCAR Digit Assets Service Hub via https://doi.org/10.5065/f8z0-0p03 (?, ?).

### Acknowledgments

Dong Lin is supported by the Advanced Study Program (ASP) Postdoctoral Fellowship of National Center for Atmospheric Research (NCAR). NCAR is sponsored by National Science Foundation (NSF). This work is supported by NASA GCR grant 80NSSC17K0013, DRIVE Science Center for Geospace Storms (CGS) under grant 80NSSC20K0601, LWS grants 80NSSC20K0356, 80NSSC19K0080, 80NSSC17K0679, and 80NSSC20K0199. CSH at the Air Force Research Laboratory is supported by NASA grants 80HQTR20T0015 and 80HQTR20T0016. MO is supported by NASA LWS grant 80NSSC19K0080. KS is supported by NASA 80NSSC19K0241 and 80NSSC20K1833. QW is supported by NASA LWS 80NSSC20K0199, NNX17AG69G, and 80NAAC21K0014. YZ is supported by NASA grant 80NSSC20K0354. We would like to acknowledge high-performance computing support from Cheyenne (doi:10.5065/D6RX99HX) provided by NCAR's Computational and Information Systems Laboratory. Dong Lin is thankful to Dr. Gang Lu for the internal review. The OMNI data are available at https://cdaweb.gsfc.nasa.gov/index.html/. The DMSP SSJ and SSIES data are obtained from http://cedar.openmadrigal.org/.

## References

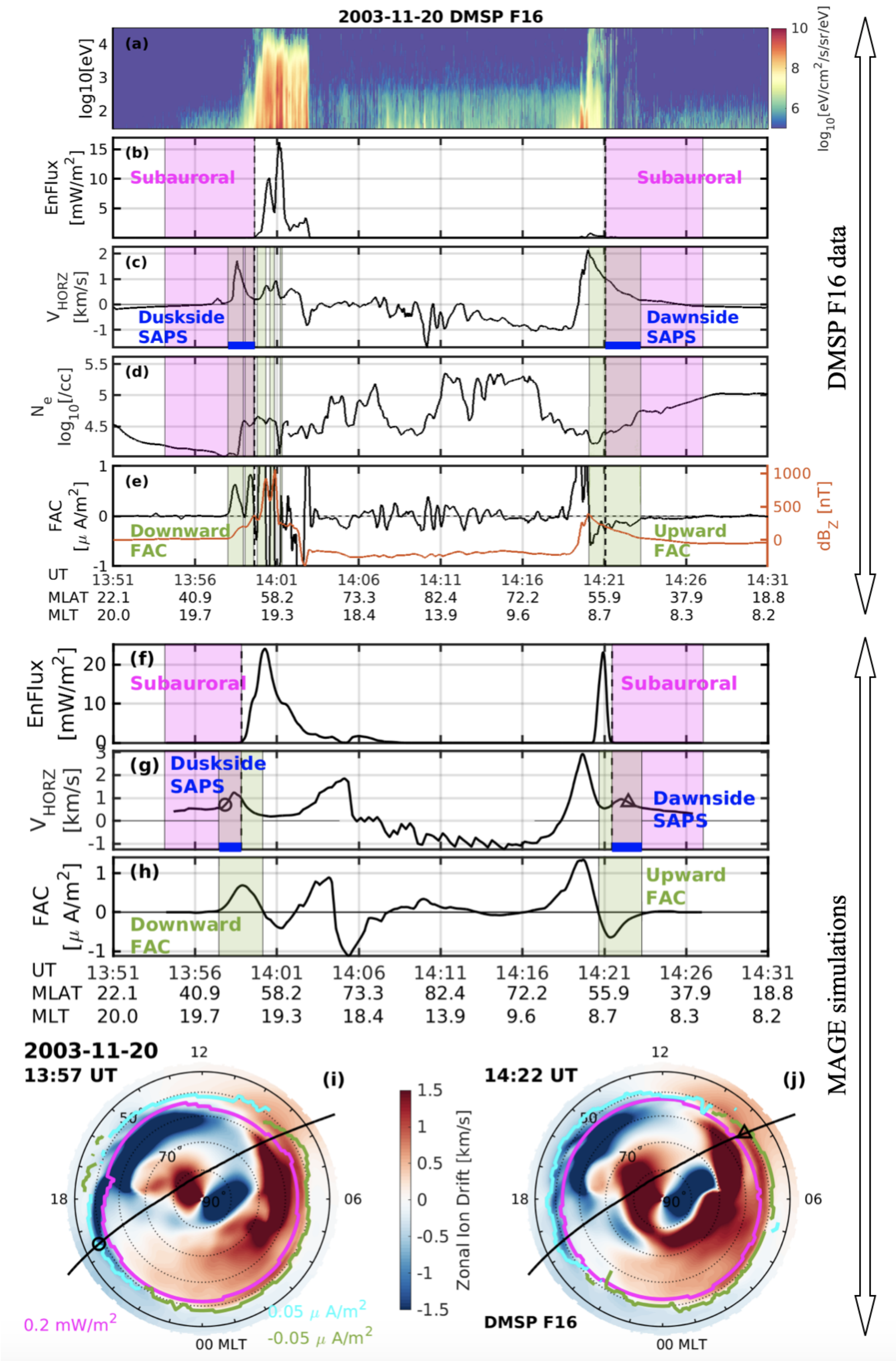


**Figure 2.** (a-e) SAPS observed by DMSP F16 and (f-j) simulated by the MAGE model from 13:51 UT to 14:31 UT. (a) Electron precipitation energy spectrum. (b) Integrated electron precipitation energy flux ($EnFlux$). (c) Cross track ion drift velocity ($V_{HORZ}$). (d) Electron density. (e) Cross-track horizontal magnetic perturbation (orange) and the derived FAC density (black). (f-h) MAGE simulation results of $EnFlux$, $V_{HORZ}$, and FAC sampled along DMSP F16 trajectory. (i-j) Zonal ion drift velocity distributions at 13:57 UT and 14:22 UT in the northern hemisphere ionosphere viewed from the top of the north pole. The trajectory of DMSP F16 during this polar cap crossing is shown by the black curves in (i-j), with the black circle and triangle indicating the location at those two UTs. The magenta, cyan, and dark green curves in (i-j) in

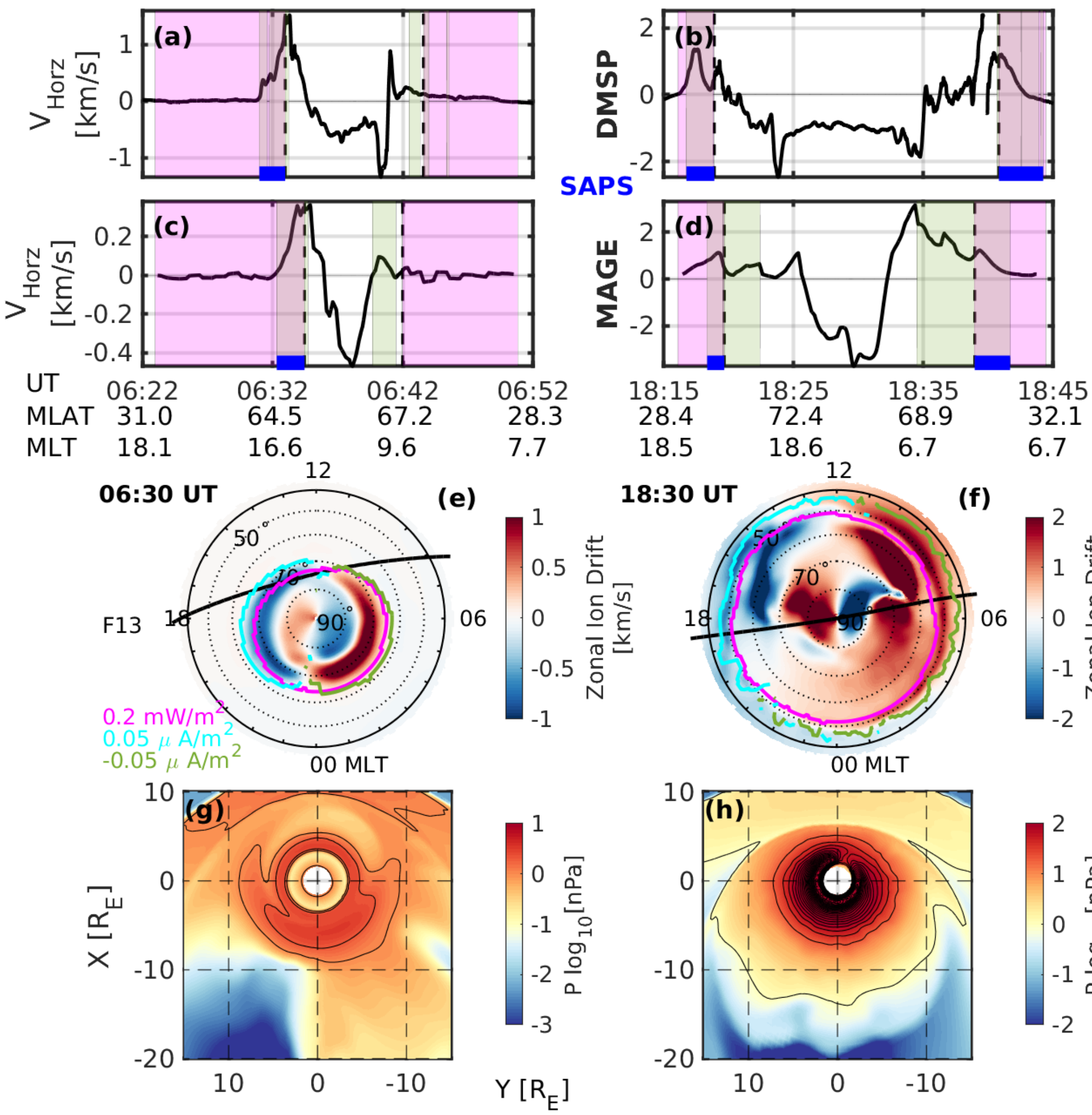


**Figure 3.** Comparison of SAPS between storm time and before the storm. (a-b) DMSP F13 measurements of $V_{Horz}$ during 06:22-06:52 UT, and during 18:15-18:45 UT. (c-d) MAGE simulation results of $V_{Horz}$ sampled along DMSP F13 trajectories during the two intervals. (e-f) MAGE simulation results of zonal ion drift in the northern hemispheric ionosphere at 06:30 UT and 18:30 UT, respectively. (g-h) Plasma pressure distribution in the magnetospheric equatorial plane at 06:30 UT and 18:30 UT on a logarithm scale.

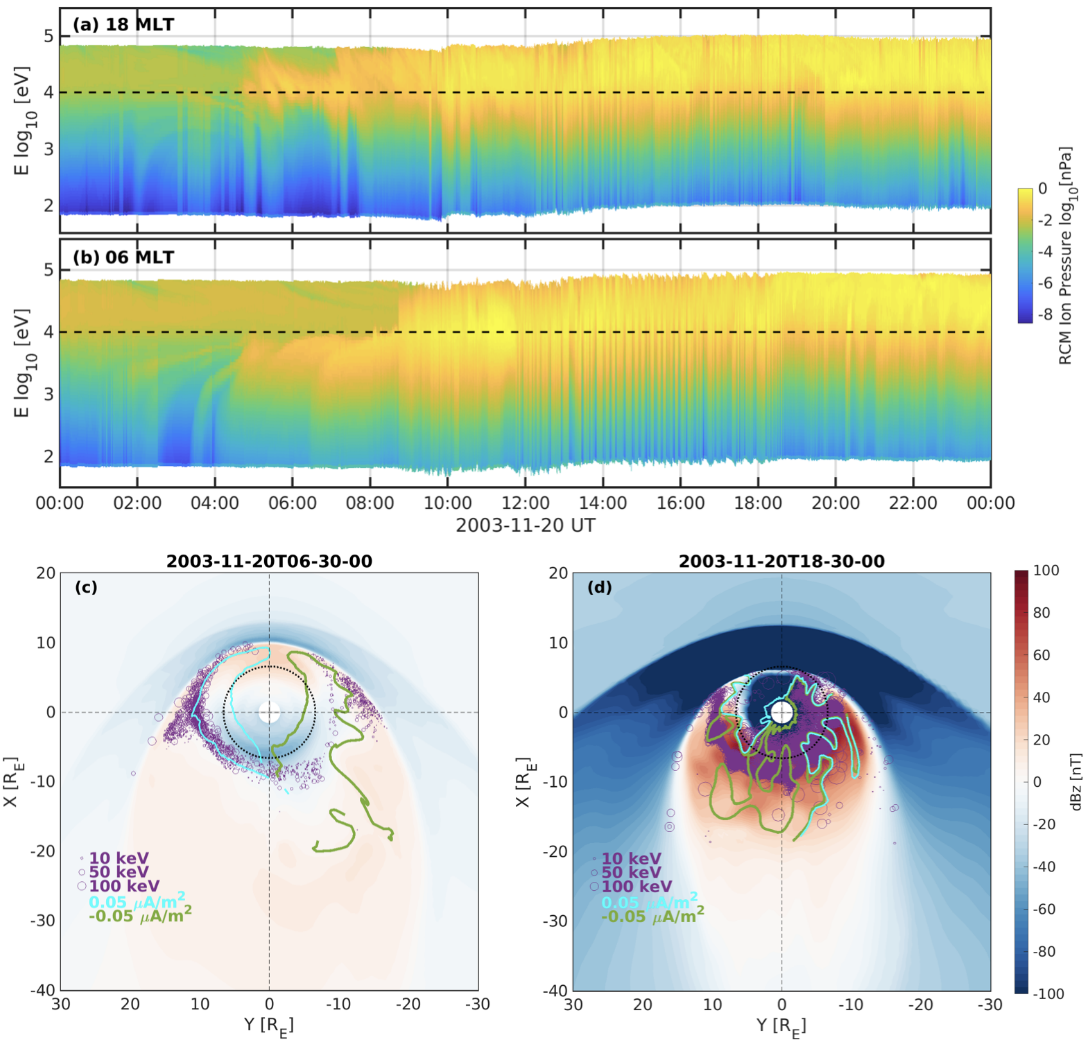


**Figure 4.** (a-b) Ring current pressure sampled at the geosynchronous orbit at 18 MLT and 06 MLT. (c-d) Equatorial distributions of test particle protons 30 minutes after they were released at 6 UT and 18 UT. The colorbar shows residual magnetic field $B_Z$ with dipole background subtracted. The green and cyan curves are ionospheric boundaries of upward and downward FACs, respectively, mapped from the northern hemisphere along geomagnetic field lines.

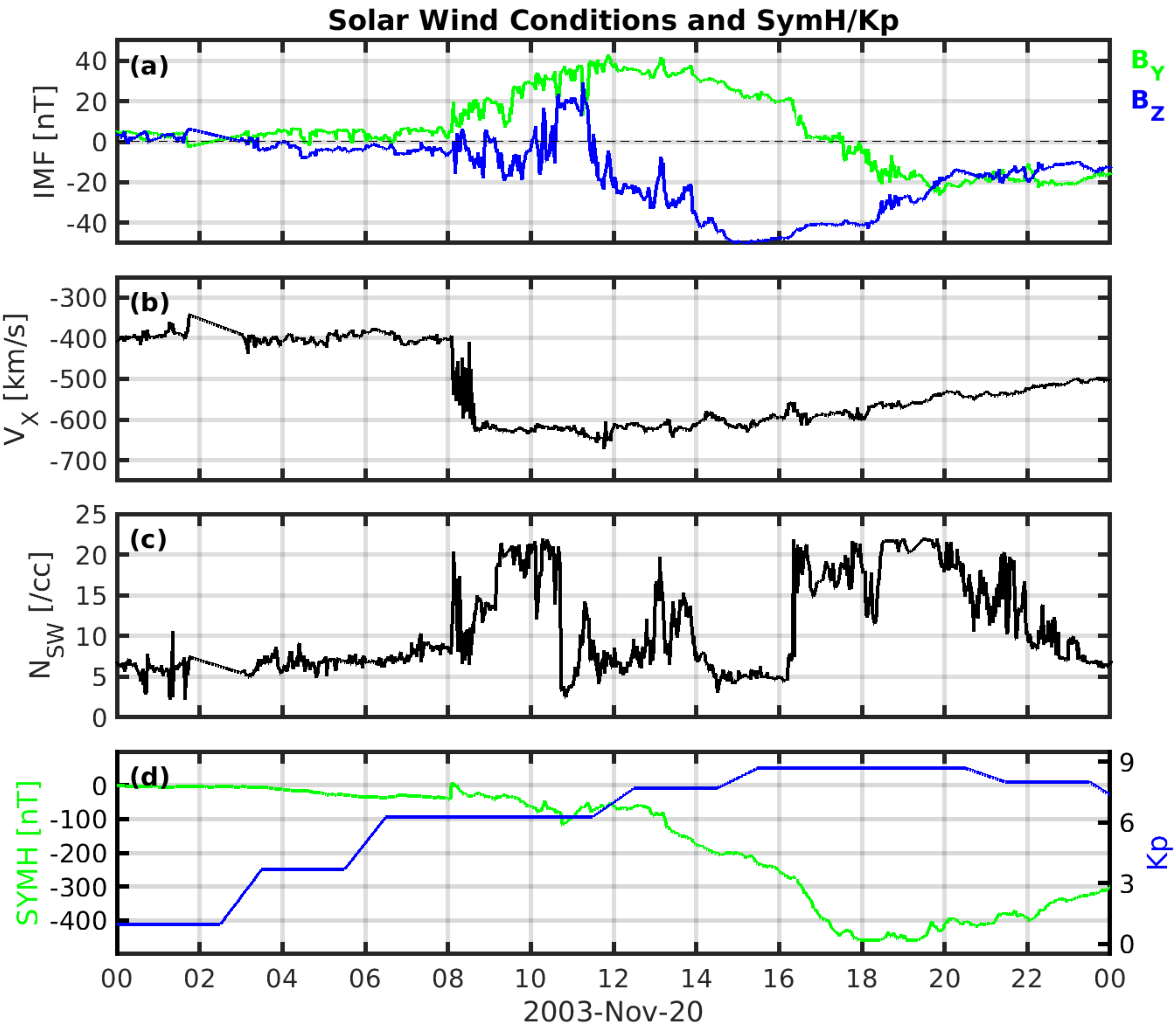

Solar Wind Conditions and SymH/Kp
(a)
(b)
(c)
(d)
IMF [nT]
B_Y
B_Z
V_X [km/s]
N_SW [/cc]
SYMH [nT]
Kp
40
20
0
-20
-40
-300
-400
-500
-600
-700
25
20
15
10
5
0
-100
-200
-300
-400
9
6
3
00
02
04
06
08
10
12
14
16
18
20
22
2003-Nov-20

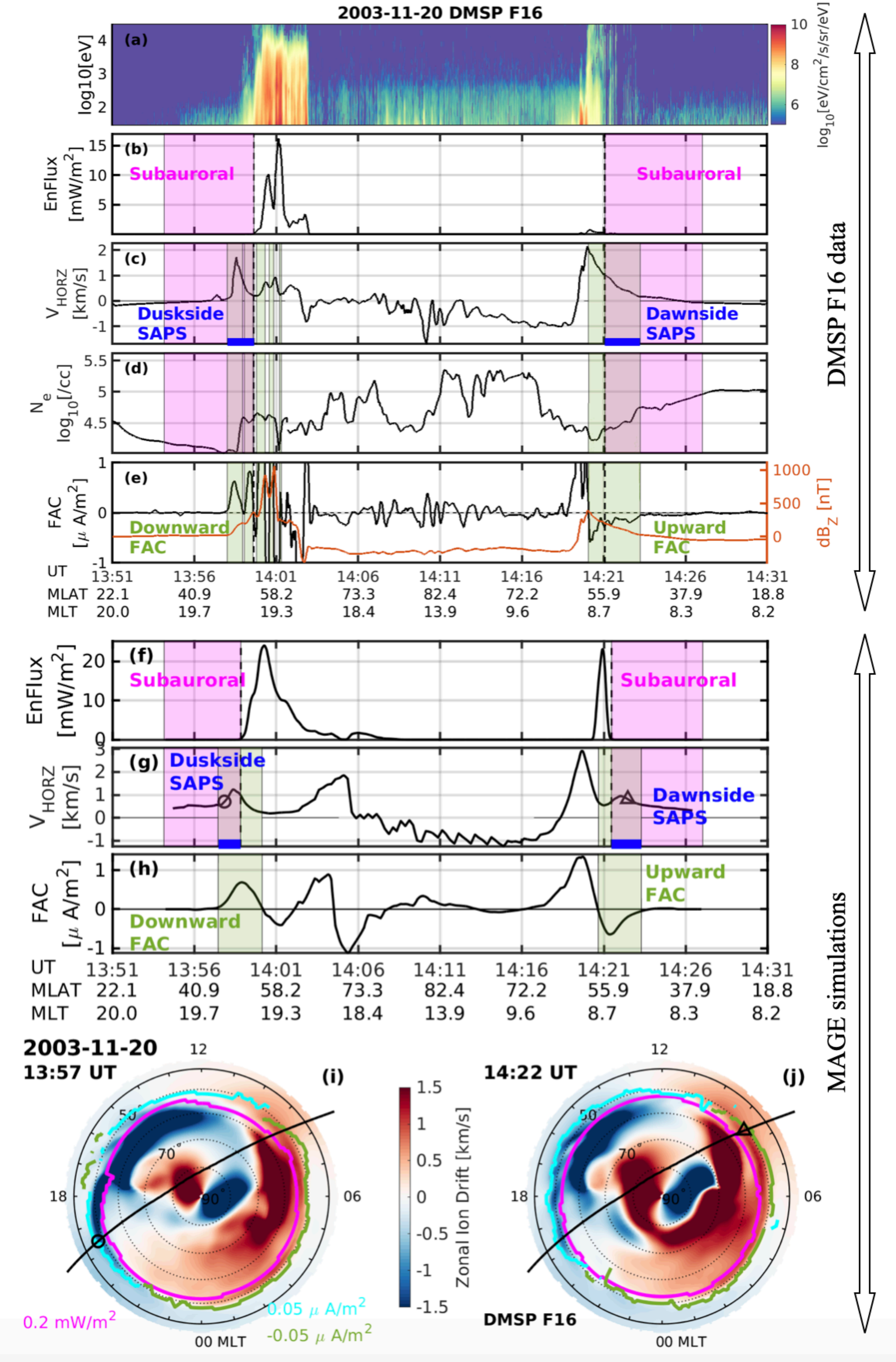

2003-11-20 DMSP F16
(a)
log10[eV]
log10[eV/cm2/s/sr/eV]
(b)
EnFlux [mW/m2]
Subauroral
Subauroral
(c)
VHORZ [km/s]
Duskside SAPS
Dawnside SAPS
(d)
Ne log10[/cc]
(e)
FAC [μ A/m2]
dBZ [nT]
Downward FAC
Upward FAC
UT 13:51 13:56 14:01 14:06 14:11 14:16 14:21 14:26 14:31
MLAT 22.1 40.9 58.2 73.3 82.4 72.2 55.9 37.9 18.8
MLT 20.0 19.7 19.3 18.4 13.9 9.6 8.7 8.3 8.2
DMSP F16 data
(f)
EnFlux [mW/m2]
Subauroral
Subauroral
(g)
VHORZ [km/s]
Duskside SAPS
Dawnside SAPS
(h)
FAC [μ A/m2]
Downward FAC
Upward FAC
UT 13:51 13:56 14:01 14:06 14:11 14:16 14:21 14:26 14:31
MLAT 22.1 40.9 58.2 73.3 82.4 72.2 55.9 37.9 18.8
MLT 20.0 19.7 19.3 18.4 13.9 9.6 8.7 8.3 8.2
MAGE simulations
2003-11-20
13:57 UT
(i)
12
18
06
00 MLT
Zonal Ion Drift [km/s]
14:22 UT
(j)
12
18
06
00 MLT
0.2 mW/m2
0.05 μ A/m2
-0.05 μ A/m2
DMSP F16

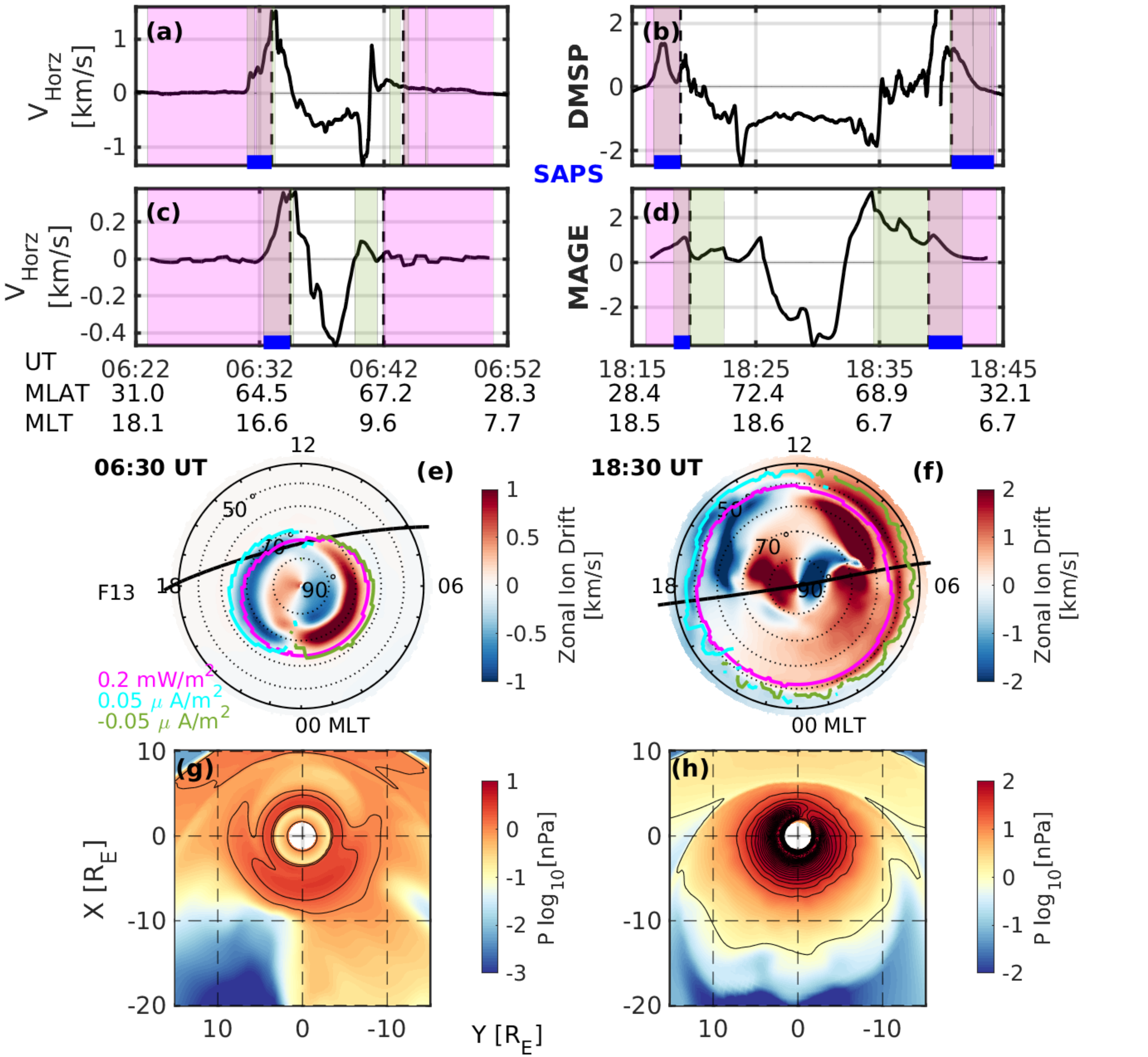

(a)
V_Horz [km/s]
(b)
DMSP
SAPS
(c)
(d)
MAGE
UT 06:22 06:32 06:42 06:52 18:15 18:25 18:35 18:45
MLAT 31.0 64.5 67.2 28.3 28.4 72.4 68.9 32.1
MLT 18.1 16.6 9.6 7.7 18.5 18.6 6.7 6.7
06:30 UT
(e)
F13
12
18
06
00 MLT
50°
70°
90°
0.2 mW/m^2
0.05 μ A/m^2
-0.05 μ A/m^2
Zonal Ion Drift [km/s]
18:30 UT
(f)
(g)
(h)
X [R_E]
Y [R_E]
P log_10[nPa]

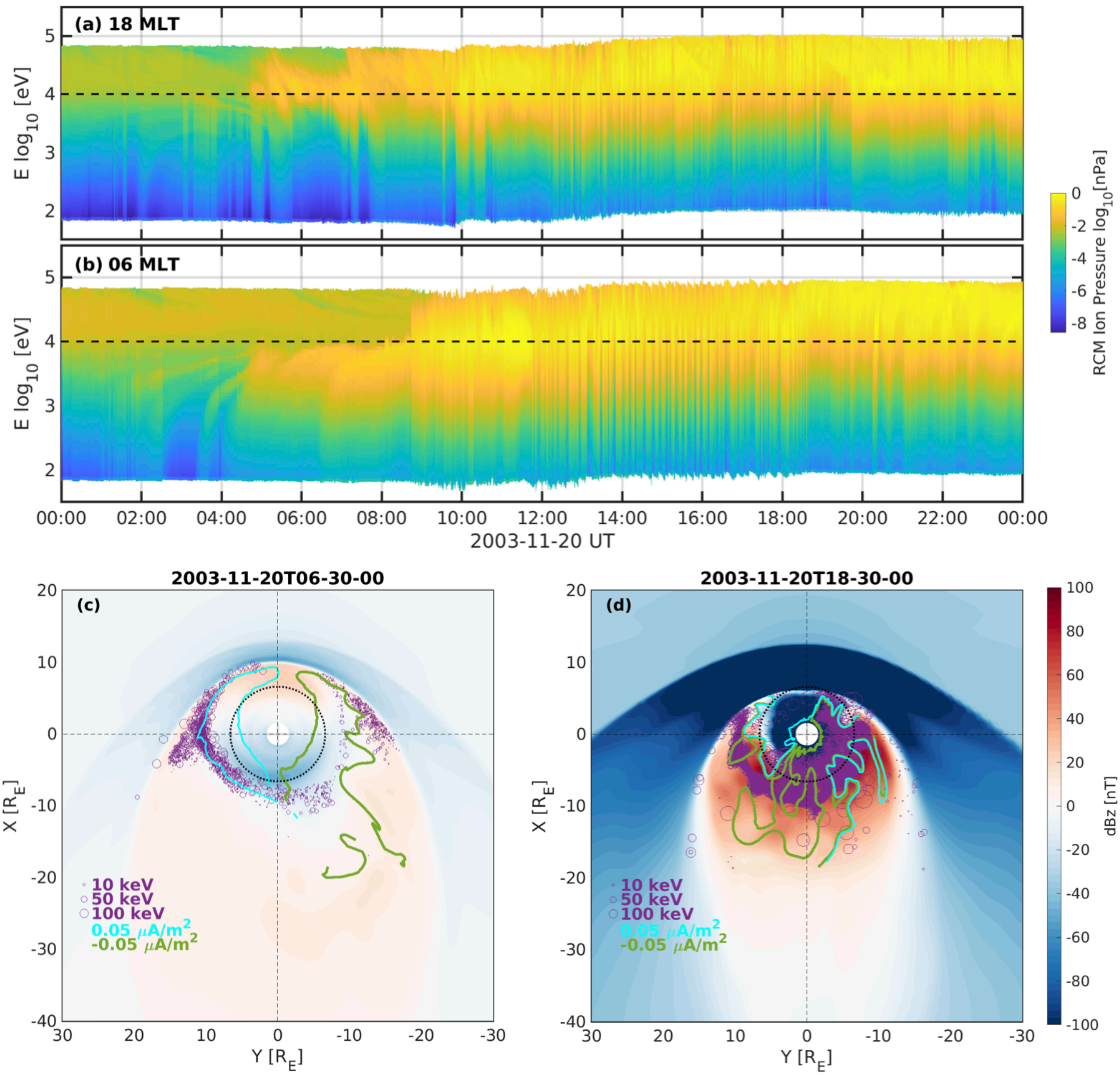

(a) 18 MLT
(b) 06 MLT
E log10 [eV]
RCM Ion Pressure log10[nPa]
2003-11-20 UT
00:00
02:00
04:00
06:00
08:00
10:00
12:00
14:00
16:00
18:00
20:00
22:00
00:00
2003-11-20T06-30-00
2003-11-20T18-30-00
(c)
(d)
X [RE]
Y [RE]
dBz [nT]
10 keV
50 keV
100 keV
0.05 μA/m2
-0.05 μA/m2